RSC Advances

PAPER

View Article Online
View Journal | View Issue

Cite this: *RSC Adv.*, 2025, **15**, 21037

Valorization of a Cr-MOF/polymer composite for the determination of imidacloprid in fish *via* dispersive solid-phase microextraction

Muhammad Hayat,[a] Nadeem Raza,*[b] Suryyia Manzoor,*[a] Yasmeen Irshad,[a] Ramika Javaid,[a] Abdul Waqar Rajput[c] and Faisal K. Algethami[b]

Imidacloprid (IMI) is increasingly prevalent in different environmental segments and has emerged as a possible threat to the ecosystem and human health. Therefore, a sustainable, effective, and eco-friendly approach is necessary for IMI detection. This study reports a new Cr-MOF/polymer composite for the detection of IMI in fish using the dispersive solid-phase microextraction method. This Cr-MOF/polymer composite was synthesized by combining a Cr-MOF with functional monomers, including acrylonitrile and vinyl acetate, to improve the selective absorption of IMI from complex fish sample matrixes. The Cr-MOF/polymer composite was well characterized through SEM, BET analysis, FTIR analysis, and TGA. Kinetics and isotherm analyses suggested that the sorbent's adsorption performance was due to H-bonding. Adsorption data fitted well with the Freundlich model ($R^2 = 0.991$), indicating physisorption, following pseudo-first-order kinetics ($\chi^2 = 1.86$, $R^2 = 0.996$). The LOD and LOQ for IMI in fish samples determined through HPLC were 0.004 and 0.012 μg g^{-1}, respectively. Reusability tests confirmed that the Cr-MOF/polymer composite could be used for over six consecutive cycles. These findings underscore the practical importance of the developed composite in environmental monitoring and enhancing food safety to safeguard public health.

Received 23rd March 2025
Accepted 8th June 2025

DOI: 10.1039/d5ra02053k

rsc.li/rsc-advances

1. Introduction

Aquatic products, which are significant food sources, are gaining increasing attention because of their positive health benefits and ability to prevent chronic diseases.[1] However, ensuring hygienic safety remains challenging owing to risks of spoilage, persistent pollutants, and lipid oxidation.[2,3] The world has switched to natural alternatives, such as essential oils and plant extracts, which can provide antioxidants and antimicrobial agents and offer extended shelf life, thereby addressing safety and health concerns in the aquatic food industry.[4,5] The global popularity of fish as a vital component of a healthy diet has surged in recent decades, even in regions where fish is not traditionally consumed.[6] Seafood, rich in long-chain n-3 polyunsaturated fatty acids, iodine, selenium, and vitamins (A and D), provides significant health benefits.[7] Numerous anthropogenic activities lead to the release of different contaminants into aquatic ecosystems, endangering aquatic life, degrading environmental quality, and making water bodies unfit for human consumption.[8–10] However, persistent organic pollutants, particularly pesticides in aquatic products, are threatening to human and animal life.[11] These environmental residues can potentially concentrate in fish muscle tissues and can cause endocrine disruptions, neurotoxicity, and cancer.[12] Pesticides are frequently utilized to control pests to increase crop yields, but their unmanaged use may lead to contamination of the ecosystem.[13] Runoff water from pesticide-treated crops contaminates rivers and seas, contributing to the bioaccumulation of harmful substances in aquatic organisms.[14]

Imidacloprid (IMI), a neonicotinoid insecticide, primarily targets sucking insects, like aphids and whiteflies, by disrupting their nervous systems through selective binding to nicotinic acetylcholine receptors.[15] IMI can penetrate plant tissues and potentially contaminate water systems through runoff, leading to bioaccumulation in diverse aquatic organisms, including fish.[16] Pesticides can accumulate in fish and then enter the food chain, ultimately causing severe health impacts in humans. For instance, exposure to pesticides has been associated with endocrine disruption, obesity, cancer, and other illnesses in humans.[17]

Currently, diverse instrumental approaches, including high performance liquid chromatography (HPLC),[18] tandem techniques, such as HPLC-tandem mass spectrometry (HPLC-MS/MS),[19] and gas chromatography-tandem mass spectrometry (GC-MS/MS)[20] have been reported[21] for the investigation of IMI in various matrixes. However, the fate of IMI analysis heavily relies

[a]*Institute of Chemical Sciences, Bahauddin Zakariya University, Multan, Pakistan. E-mail: suryyia.manzoor@bzu.edu.pk*

[b]*Department of Chemistry, College of Science, Imam Mohammad Ibn Saud Islamic University (IMSIU), Riyadh, Kingdom of Saudi Arabia. E-mail: nrmostafa@imamu.edu.sa*

[c]*College of Textile Engineering, Bahauddin Zakariya University, Multan, Pakistan*

on the extraction and preconcentration of IMI residues in highly complex matrixes, such as fruits, vegetables, and the tissues of animals.[22] To improve the selectivity and accuracy of these chromatographic techniques, the extraction and preconcentration of targets are usually executed through physical adsorption owing to its several attributes in terms of simplicity and convenience,.[23] This flexible method allows for quick separation with little sample preparation, making the overall process more efficient. Also, the ability to reuse adsorbent materials helps with sustainability, and its scalability ensures that it can be deployed for different analytical needs.[24] The extraction of IMI residues directly from fish parts is difficult because of its complex matrix effect and low concentration. Consequently, an accurate and reliable method for the preparation of samples could assist in resolving the aforementioned issues. Various methods, including solid-phase extraction (SPE), solid-phase microextraction (SPME), magnetic solid-phase extraction (MSPE), and Quick, Easy, Cheap, Effective, Rugged, Safe (QuEChERS) have been deployed for IMI preconcentration and its subsequent analytical detection.[25,26] Dispersive solid-phase microextraction (DSPME) has gained much attention due to its several benefits, including easy to operate, no restriction on adsorbent conditioning, and enhanced target adsorption on the sorbent surface. In recent years, for the adsorption of IMI residues, a wide range of synthetic and/or commercial adsorbents have been proposed, including resorcinol formaldehyde carbon cryogel,[27] multi-walled carbon nanotubes,[28] polymers,[29] magnetic nanoparticles,[30] agro-waste biosorbents,[31] and magnetic three dimensional graphene,[32] as well as metal–organic frameworks (MOFs).[33] Among these sorbents, MOFs have gained significant interest owing to their large surface area, porous structure, tunability, easy modification, and exceptional mechanical and thermal stability.[34] The solvothermal approach is preferred in MOF synthesis due to the fact that the reactions are conducted in sealed vessels at higher temperatures and pressures, resulting in a better solubility of the reactants and the formation of homogenous MOF crystals with large surface areas and porosity.

However, the combination of MOFs with appropriate imprinting polymers can further enhance these properties by improving the material's interaction with specific target molecules, thereby optimizing separation processes and increasing the overall efficiency.[35]

This study was focused on developing a chromium (Cr)-MOF/polymer composite for the detection of IMI in fish using DSPME. To the best of our knowledge, no such study has been previously reported. DSPME was selected based on its notable extraction efficiency and minimal sample solution consumption. The Cr-MOF/polymer composite was characterized using numerous well-known analytical techniques, including Fourier transform infrared spectroscopy (FTIR), thermogravimetric analysis (TGA), Brunauer–Emmett–Teller (BET), scanning electron microscopy (SEM) and energy-dispersive X-ray spectroscopy (EDX). Comprehensive optimization of various experimental variables, such as the concentration of IMI, pH, time of contact, and dose of sorbent, was achieved through batch adsorption studies, ensuring the effectiveness of the suggested approach for IMI estimation in fish. This study aimed to help improve the quality control and quality assurance management of food to ensure high-quality food standards through the efficient detection of IMI in food samples.

2. Materials and methods

2.1. Chemicals and reagents

Acetonitrile (99.9%) was obtained from Riedel-deHaën (Germany). The monomer vinyl acetate (99.9%) and initiator benzoyl peroxide (99%) were purchased from Daejung (Korea). Ethylene glycol methacrylate (>98%) and acrylonitrile (>99.5%) were obtained from Merck (Germany). Terephthalic acid (98%) and chromium nitrate (98%) were purchased from Duksan (Korea).

2.2. Synthesis of Cr-MOF

Cr-MOF was synthesized using the solvothermal method.[36] In brief, a mixture of chromium nitrate (12.03 g) and terephthalic acid (4.92 g) was combined with DMF (20 mL) in a glass beaker. The mixture was sonicated for 20 min, then transferred into an autoclave and placed in a furnace at 150 °C for 18 h. After that, the mixture was allowed to cool at room temperature, and light greenish precipitates were obtained after centrifuging at 4000 rpm for 15 min. The obtained product was then washed with DMF through sonication for 10 min. Finally, the material was dried to yield a greenish powder.

2.3. Synthesis of the Cr-MOF/polymer composite

The Cr-MOF/polymer composite was prepared using a thermal polymerization method. Briefly, acrylonitrile (0.53 mL) and vinyl acetate (0.83 mL) were mixed with 1.69 mL of the cross-linker ethylene glycol dimethacrylate (EGDMA) and 90 mg of the previously prepared Cr-MOF. This mixture was dissolved in 20 mL acetonitrile in a flask and subsequently 0.10 g of the initiator benzoyl peroxide was added. The resulting mixture was then sonicated for 5 min in a water bath while nitrogen gas was continuously purged for an additional 15 min. After sealing the flask tightly, the solution mixture was heated at 80 °C for 1 day, resulting in the formation of a cloudy solid polymer. After the complete reaction, the polymer product was washed with deionized H_2O and then dried in an oven at 100 °C for 1 h.

2.4. Characterization of the Cr-MOF/polymer composite

FTIR spectra of the Cr-MOF and Cr-MOF/polymer composite were measured in the scanning range of 4000–500 cm^{-1} using a Bruker Alpha II FTIR spectrometer (IFS 125HR FTIR, Germany) equipped with a single reflection diamond automated refractometer (ATR) module. The IMI concentration was assessed by measuring its absorbance at 270 nm with a Shimadzu UV-800ENG240V SOFT spectrophotometer. The surface morphology of the samples was observed using scanning electron microscopy (JEOL, JSM 5910 Japan), while energy-dispersive X-ray spectroscopy (EDX) was used to examine the sample's elemental composition. For sample preparation, gold sputtering was performed under vacuum ($\sim 10^{-3}$ Torr) using a JEOL JFC-1000E ion sputter coater. The samples (Cr-MOF and

Cr-MOF/polymer composite) were coated at 15 kV for 200 s to provide a conductive layer suitable for EDX analysis. The thermal stability of both samples was evaluated under a N_2 environment using a TGA unit (STA 8000, PerkinElmer, USA). For chromatographic analysis, an Agilent 1100 liquid chromatograph, fitted with a heated column compartment, a diode array detector, and a workstation from LC, was used. Brunauer–Emmett–Teller (BET) surface area analysis and nitrogen adsorption–desorption isotherms were obtained using a Quanta-chrome Instruments 2000-12 system, version 5.1, in the pressure range of 0.0658629–0.466542, at 77.3 K to examine the surface area and pore distribution. For all the analyses, 50 mg of each dried Cr-MOF and Cr-MOF/polymer composite sample was degassed under a nitrogen flow prior to measurement.

2.5. Determination of the point of zero charge (pHpzc)

The point of zero charge (pHpzc) refers to the pH at which the surface of an adsorbent carries no net electrical charge, meaning the number of positive and negative charges on the surface are equal. To determine the pHpzc of the Cr-MOF/polymer composite, the mass titration method was employed. In the analysis, 13 separate flasks, each containing 50 mL of 0.5 M NaCl solution, were used. To each flask, 40 mg of the Cr-MOF/polymer composite was added. The pH of these suspensions was carefully adjusted to values ranging from 1 to 13 using 0.1 M solutions of NaOH and HCl. The samples were then shaken continuously on an orbital shaker for 24 h to attain equilibrium.

After equilibration, the suspensions were filtered, and the final pH of each filtrate was measured using a benchtop pH meter (HI-2211, Hanna Instruments, UK). A graph of the initial pH *versus* final pH was plotted to find out the pHpzc, which was the point at which the initial pH and ΔpH overlapped each other and the adsorbent must be neutral at this pH.[37]

2.6. Batch adsorption studies

The IMI sample's absorbance was measured using a Shimadzu UV-800ENG240V SOFT spectrophotometer between 200 and 400 nm, with the maximum absorbance at 270 nm for determining the IMI concentration. In the adsorption experiments, 50 mg of Cr-MOF/polymer composite was added in to 50 mL IMI standard solution (50 mg L^{-1}) in test tubes, followed by sonication for 10 min. Aliquots were taken at varying time intervals (5–40 min) in order to calculate the binding capacity. Additionally, a series of standard IMI solutions were prepared that ranged in concentration from 10 to 100 mg L^{-1}, and adsorption was performed at room temperature. After agitation for 30 min, the solutions were filtered and analyzed using a UV-vis spectrophotometer, and their absorbance was noted. The binding capacity was calculated using eqn (1).

$$q_e = \frac{(C_i - C_f)}{M} \times V \quad (1)$$

where q_e is the binding capacity, C_i and C_f are the IMI's respective initial and final concentrations in solution, V is the solution volume, and M is the mass of the Cr-MOF/polymer composite.

In the next step, 50 mg L^{-1} IMI solutions were prepared in flasks with the pH value adjusted in the range from 3 to 10 using 0.1 M solutions of HCl and NaOH. Then, 50 mg Cr-MOF/polymer composite was added to 10 mL IMI solution and shaken on an orbital shaker for 20 min. Afterwards, the absorbance of the IMI solutions at different pH levels was measured at 270 nm.

2.7. Performance of the Cr-MOF/polymer composite for the adsorptive removal of imidacloprid from fish samples

Five samples of Rohu fish (*Labeo rohita*) of varying sizes with lengths ranging from 44 to 58 cm and weights between 1.2 and 2.0 kg were bought from a local market in the vicinity of Multan district, Punjab, Pakistan. The heads and tails were carefully removed, and all the other parts of the fish were properly cleaned. These cleaned fish were then minced into a uniform mixture. The whole fish, excluding the heads, central bones, and tails, were blended for 10 min in a Braun blender FP3010, ensuring the sample was thoroughly homogenized. Next, 5.0 g of the blended fish samples were weighed and transferred to centrifuge tubes, which were then spiked at three distinct concentrations: 1, 3, and 5 μg L^{-1} with standard IMI solutions. The solution mixtures were then sonicated for 10 min followed by centrifugation. The supernatant was collected, and subsequently, 50 mg Cr-MOF/polymer composite was added into each one. The mixtures were allowed to stir for 30 min to facilitate adsorption and then centrifuged for 3 min at 6000 rpm, to separate the adsorbent from the rest of the solution.[38]

To desorb the adsorbed IMI on the Cr-MOF/polymer composite, 5 mL ethanol was introduced to the sorbent, which was then agitated for 20 min. The desorbed IMI was then analyzed using HPLC-DAD. The stationary phase of a C_{18} column (5 μm, 250 × 4.6 mm, Agilent, USA) was utilized, while the mobile phase consisted of a mixture of ACN and HPLC-grade H_2O (50 : 50 (v/v)), which was employed at a 0.8 mL min^{-1} constant flow rate. The mobile phase pH was carefully shifted to 7.0 ± 0.2 using dilute 0.1 M solutions of HCl and NaOH to ensure optimal separation and the accurate quantification of IMI.

The percentage recovery of the spiked samples was determined using eqn (2).

$$\%\ \text{Recovery} = \frac{(C_{found} - C_{real})}{C_{added}} \times 100 \quad (2)$$

The % recovery indicates the efficiency of the Cr-MOF/polymer composite in adsorbing imidacloprid (IMI) by comparing the amount of IMI recovered after the adsorption process to the amount that was initially added. In eqn (2), C_{found} refers to the concentration of IMI found in the sample after the adsorption, C_{real} is the real concentration of IMI originally present in the sample, and C_{added} is the amount of IMI that was added for the recovery test. The difference between C_{found} and

C_{real} represents the amount of IMI successfully adsorbed by the MOF-based sorbent.[39]

2.8. Regeneration studies

A sorbent's cost-effectiveness is determined by its ability to be reused in multiple extraction cycles without sacrificing its efficiency.[40] Regeneration experiments were performed to assess the reusability of the Cr-MOF/polymer composite. For the first cycle, 50 mg of the composite was dispersed into 35 mL IMI standard solution (50 mg L^{-1}) at ambient temperature. The resulting solution was agitated for 30 min at 100 rpm, and after that the target pesticide concentration in the filtrate was determined utilizing a UV-vis spectrophotometer. IMI was quantified at its maximum absorption wavelength of 270 nm. After adsorption, the Cr-MOF/polymer composite was recovered through centrifugation, ensuring minimal sorbent loss, then rinsed multiple times with ethanol and allowed to dry in an oven at 70 °C. The obtained regenerated composite was reused in each subsequent cycle. Six adsorption–desorption cycles were performed to assess the composite's stability and efficiency across multiple uses. In a similar manner, the regeneration analyses were performed on fish samples following the procedure outlined in Section 2.6, with an additional spiking step using a 50 mg L^{-1} solution.

3. Results and discussion

3.1. Adsorption mechanism

The effectiveness of adsorption techniques is strongly dependent on the extent of the analyte–composite interaction. This interaction is crucial for effectively separating and keeping the target analytes from the highly challenging sample matrixes.[41] In the present work, we successfully synthesized a Cr-MOF/polymer composite with remarkable porosity and a high specific surface area. Since the adsorption process involves the interactions between the target pesticide and an adsorbent, this necessitates by the presence of a certain functionality on an adsorbent surface. To this end, the currently developed Cr-MOF/polymer composite comprised functional monomers that included acrylonitrile, vinyl acetate, and a crosslinking agent (EGDMA).

The Cr-MOF with vinyl acetate contributes ester groups that can form hydrogen bonds with the amino groups on IMI (Fig. 1), additionally, the composite's high porosity and specific surface areas provide ample sites for the physical adsorption of IMI molecules.[42]

3.2. Characterization

3.2.1. FTIR analysis. FTIR spectra (Fig. 2) of both Cr-MOF and Cr-MOF/polymer composite were acquired in the 4000–500 cm^{-1} range. The FTIR analysis revealed distinct peaks confirming the presence of various functional groups. The prominent absorption peak at 1737 cm^{-1} confirmed the presence of the carbonyl group (C=O), while the small peak at 3616 cm^{-1} was assigned to the hydroxyl group. The peak at 1160 cm^{-1} was attributed to the CN group, while peaks for the C–H stretching vibrations of CH_3 and unsaturated systems (sp^2 hybridization) appeared at 2970 and 3041 cm^{-1}, respectively. A peak for stretching vibration due to the metal–oxygen bond could be observed at 570 cm^{-1}.[43,44] The peak at 2833 cm^{-1} was assigned to C–O, while the weak peak at 869 cm^{-1} represented the vinyl group. The presence of these functional groups in the

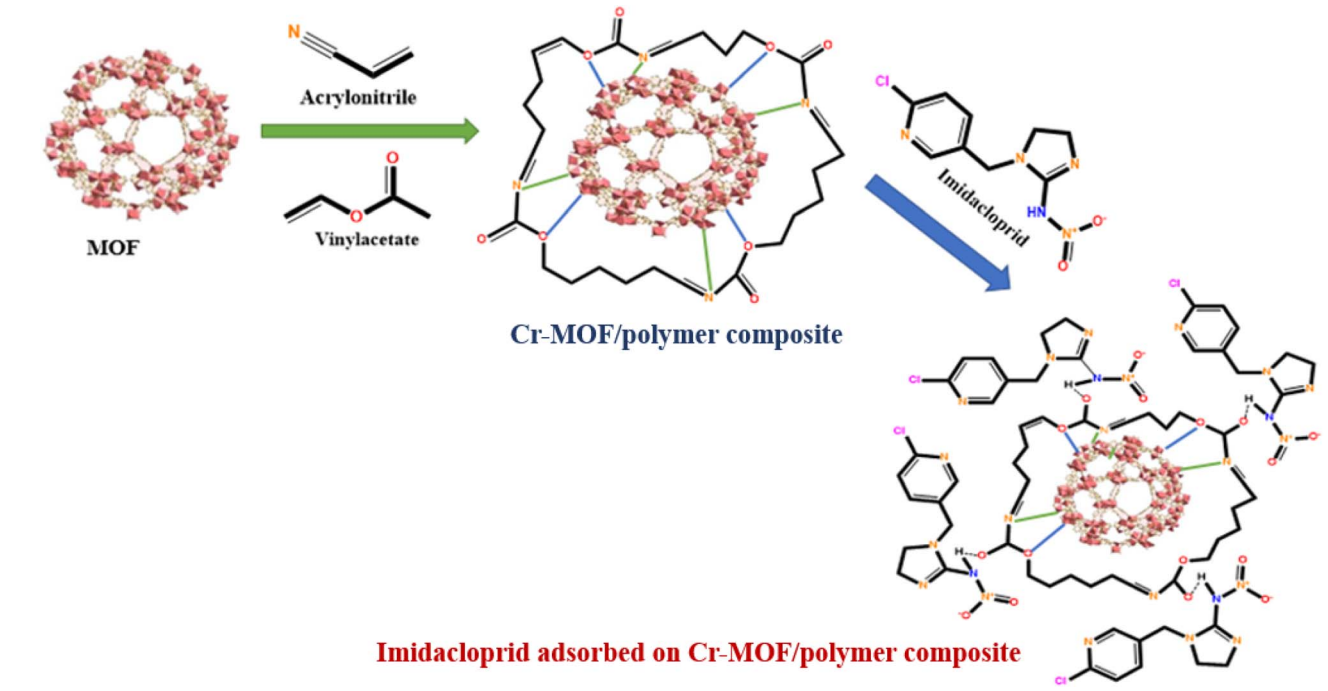

Fig. 1 Schematic of the synthesis of Cr-MOF/polymer composite, and its interaction with IMI.

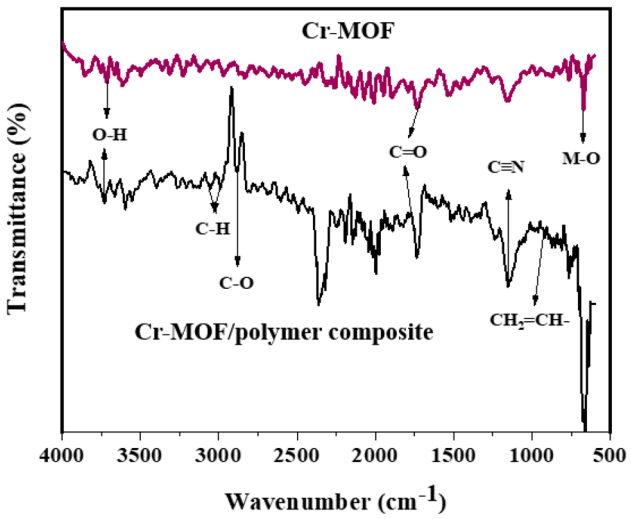

Fig. 2 FTIR spectra of Cr-MOF and Cr-MOF/polymer composite.

Cr-MOF/polymer composite could facilitate IMI adsorption on its surface.

3.2.2. SEM analysis. The Cr-MOF and Cr-MOF/polymer composite morphologies were analyzed using SEM. The SEM images (Fig. 3(a) and (b)) of Cr-MOF displayed irregular bead-like structures clustered together, whereas the Cr-MOF/polymer composite (Fig. 3(c) and (d)) consisted of spherical particles with enhanced particle interactions toward the target analyte due to the presence of surface functionalization in the monomers.

3.2.3. EDX analysis. The EDX spectra of Cr-MOF and the Cr-MOF/polymer composite (Fig. 4(a) and (b)) showed characteristic peaks for carbon, oxygen, and chromium. The EDX spectra of Cr-MOF displayed 53.81% carbon compared to the Cr-MOF/polymer composite with 81.52%. The carbon content was increased in the Cr-MOF/polymer composite due to the presence of acrylonitrile and vinyl acetate, confirming their successful incorporation. Both oxygen and chromium were detected in the Cr-MOF and the Cr-MOF/polymer composite, indicating that these elements were integral components of both materials.

3.2.4. Thermogravimetric analysis. The thermal sustainability of the synthesized Cr-MOF and Cr-MOF/polymer composite were evaluated using TGA under a nitrogen atmosphere (Fig. 5(a) and (b)). The TGA of Cr-MOF showed a multi-step weight loss, starting below 100 °C due to the removal of adsorbed water followed by DMF release between 150 and 330 °C. Major degradation occurred from 330 to 450 °C with decomposition of the organic linker (terephthalic acid), leading to the framework collapse and leaving chromium oxide residue above 450 °C. In contrast, the Cr-MOF/polymer composite exhibited a single-step weight loss of about 73% between 400 and 450 °C, corresponding to degradation of the organic components (acrylonitrile, vinyl acetate, and EGDMA). Unlike

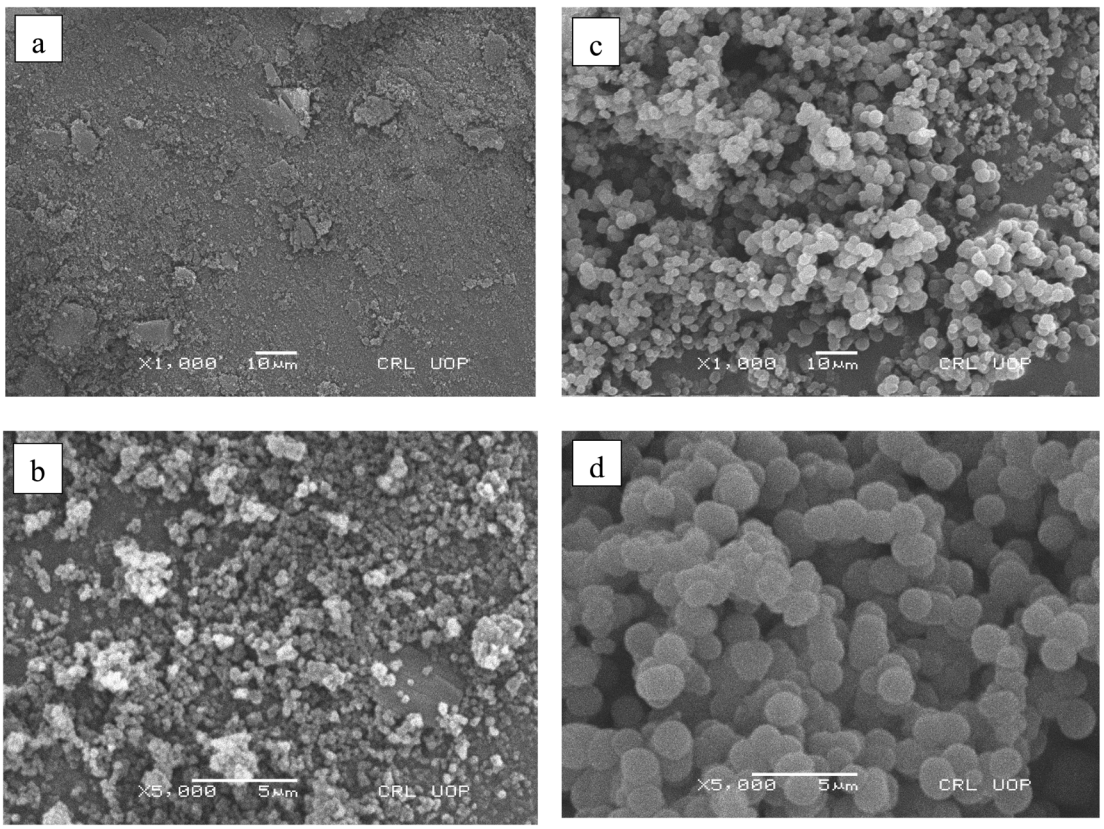

Fig. 3 SEM images of Cr Cr-MOF (a) and (b) and Cr-MOF/polymer composite (c) and (d).

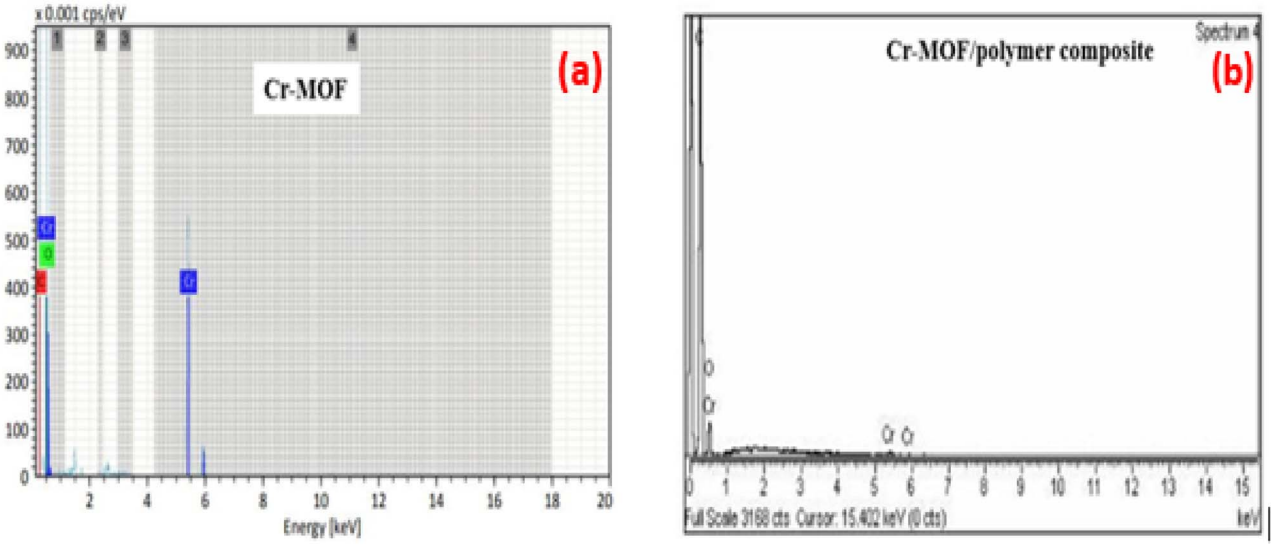

Fig. 4 EDX analysis of Cr-MOF (a) and Cr-MOF/polymer composite (b).

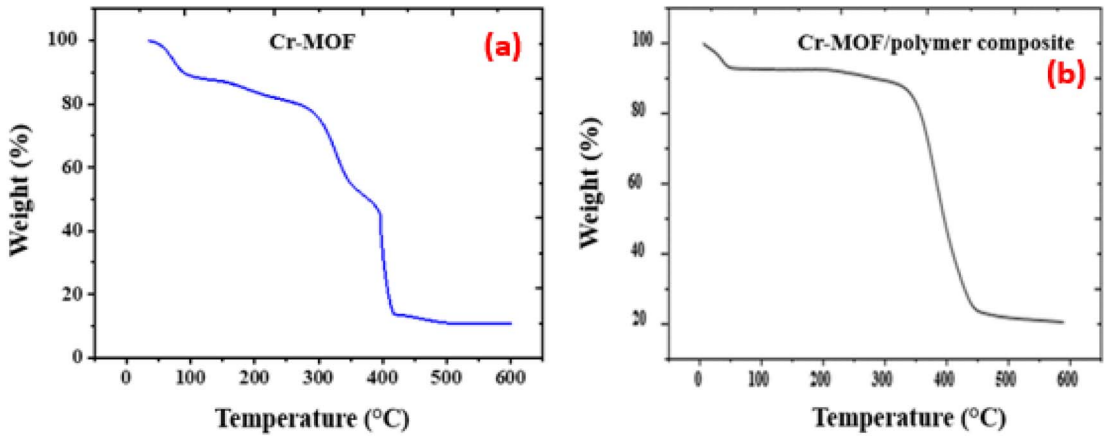

Fig. 5 Thermal stabilities of Cr-MOF (a) and Cr-MOF/polymer composite (b).

Cr-MOF, the composite lacked early solvent loss stages, showing a polymer-dominated thermal decomposition. This highlights that Cr-MOF degraded gradually with ultimate framework collapse, while the Cr-MOF/polymer composite underwent a sharp, polymer-related weight loss at higher temperatures.

3.2.5. Nitrogen adsorption/desorption. An adsorbent's surface area and pore size are crucial for its ability to retain analytes. Fig. 6(a) and (b) show the N_2 adsorption–desorption isotherms of Cr-MOF and the Cr-MOF/polymer composite, indicating that the composite exhibited a large pore size and volume relative to the pristine Cr-MOF. This increase may possibly have occurred due to the presence of the polymeric part in the composite, whose functional groups increased the distance between the metal nodes and promoted a more open framework, contributing to pore enlargement and an increased pore volume.[45] The Cr-MOF surface area was 101.70 $m^2\ g^{-1}$ with a pore volume of 0.312 cc g^{-1}. Relative to Cr-MOF, the Cr-MOF/polymer composite had a greater surface area of 191.2 $m^2\ g^{-1}$ with a mean pore volume of 0.495 cc g^{-1}.

3.3. pHpzc of the Cr-MOF/polymer composite

The pHpzc of the Cr-MOF/polymer composite was determined to be 6.9, as depicted in Fig. 7, which indicates that the Cr-MOF/polymer composite had zero-charge density on its surface at pH 6.9. Alkaline pH will impart negative charge on the Cr-MOF/polymer composite surface whereas pH below 6.9 will develop positive charge. Functional groups such as the carboxyl, nitrile, and ester groups in the Cr-MOF/polymer composite will be protonated below the pHpzc offering strong attractions for anionic analytes, while a pH level above the pHpzc will deprotonate the Cr-MOF/polymer composite, yielding strong interactions for cationic targets. Further, the presence of the above-mentioned functional groups in the Cr-MOF/polymer composite matrix strongly influenced the composite's surface acidity/basicity, causing the pHpzc to shift within the pH range of 1–13.

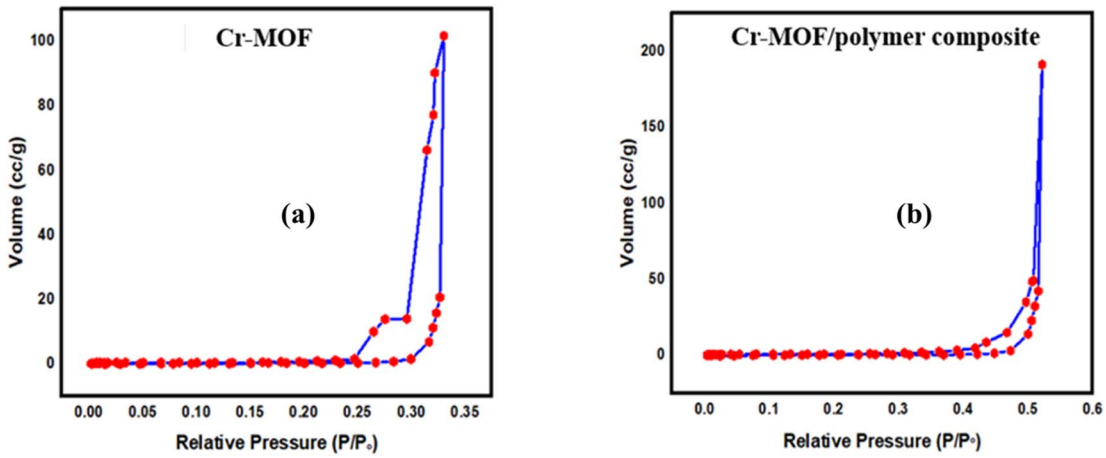

Fig. 6 Nitrogen adsorption/desorption study of Cr-MOF (a) and Cr-MOF/polymer composite (b).

3.4. Optimization of parameters

The optimization of the DSPME process for IMI using the Cr-MOF/polymer composite was evaluated across several parameters (Fig. 8(a)–(d)). The highest recovery of 97.52% occurred at a neutral pH of 7, where the optimal interaction between IMI and the sorbent was achieved. Lower pH decreased the adsorption due to the competition from H^+ ions, while higher pH led to a reduced efficiency, despite attracting positively charged IMI molecules.[46] The optimal extraction time was 30 min, yielding a recovery of 96.5%. The ideal IMI concentration was 50 mg L^{-1}, with a recovery of 96.4%, and the optimal sorbent dose was 40 mg g^{-1}, providing a recovery of 97.2%. These parameters indicate the high recovery and efficient performance of the DSPME process for IMI.

3.5. Kinetic modeling

A crucial step in developing adsorption systems includes assessing the adsorption rate of a newly synthesized sorbent.[40]

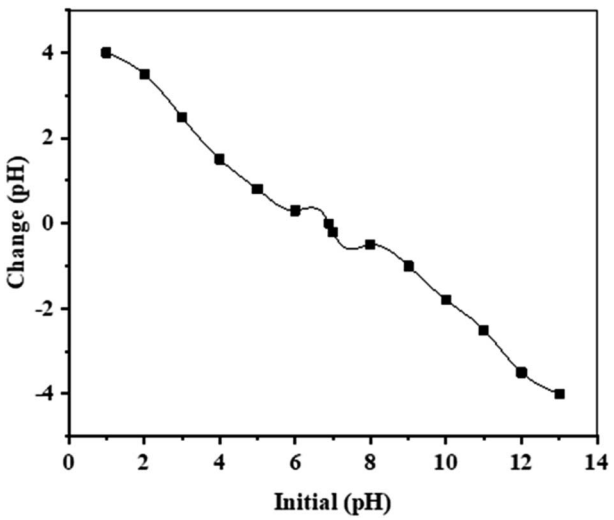

Fig. 7 pHpzc of Cr-MOF/polymer composite.

Adsorption isotherms, which provide vital information, can be utilized to predict the equilibrium concentration of an adsorbate molecule between the solid and liquid phases.[47] This helps predict the equilibrium behavior and interaction between the adsorbate and adsorbent. The present study focused on removing IMI using Cr-MOF/polymer composite, with a thorough analysis of the associated kinetics carried out through PFO, PSO, Elovich and intraparticle diffusion models. The primary objective was to unveil the fundamental mechanisms governing the adsorption phenomena.[48]

Various kinetic models, both linear and nonlinear, are commonly used in adsorption studies. Nonlinear modeling is preferred over linear regression as it provides more realistic kinetic parameters.[49] In this study, the adsorption kinetics of IMI on the Cr-MOF/polymer composite were evaluated using nonlinear models, including PFO, PSO, Elovich, and intraparticle diffusion, as shown in Fig. 9(a). Three important factors, namely R^2, q_e value, and χ^2, were employed to assess the degree of fit of the models.[50] The PFO model provided the best fit with a low χ^2 value of 1.86, high R^2 (0.996) value, and close agreement between the $q_{e(exp)}$ (55.16 mg g^{-1}) and $q_{e(cal)}$ (55.2 mg g^{-1}) values, suggesting that the adsorption followed first-order kinetics, as described in Table 1.

The adsorption rate was primarily controlled by the concentration of IMI and the available adsorption sites. The PSO model, which assumes second-order kinetics, also showed a good fit ($R^2 = 0.988$), but the q_e (62.63 mg g^{-1}) value was much higher than $q_{e(exp)}$, indicating a less accurate fit than the PFO model.[51]

The intraparticle diffusion model, which considers the penetration of adsorbate molecules into the adsorbent, showed a low R^2 (0.866) value, indicating that diffusion was not the limiting step in this case. The Elovich model, which accounts for both chemisorption and physisorption, also showed a comparable R^2 value of 0.98 but a high χ^2 value (9.7), indicating it was less suitable than the PFO model for describing the adsorption process. These findings suggest that the binding sites of the Cr-MOF/polymer composite were occupied by IMI through a physio-sorption mechanism involving physical

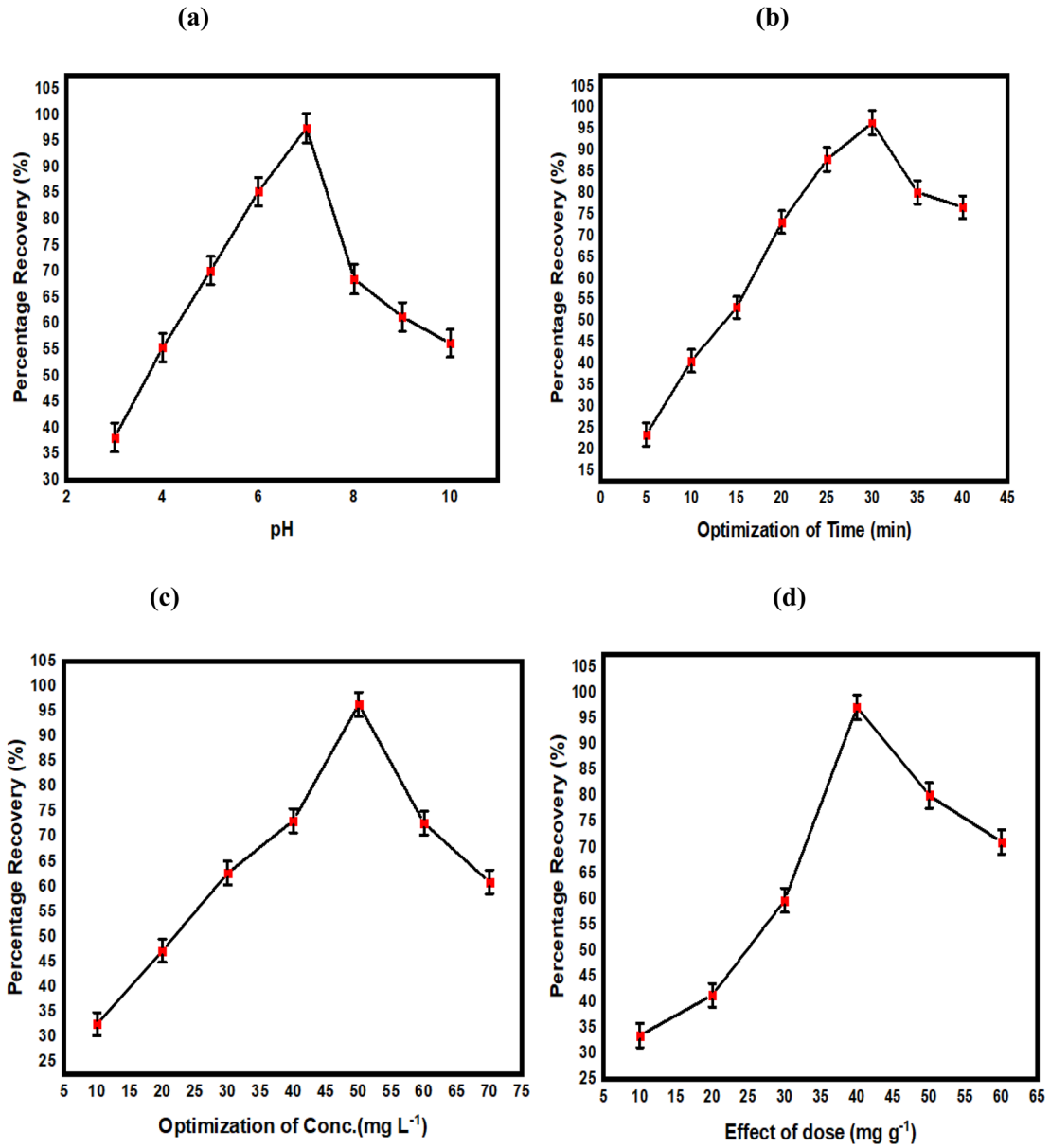

Fig. 8 Optimization of parameters for the adsorption of IMI using the Cr-MOF/polymer composite: (a) effect of pH on the IMI percentage recovery, (b) effect of contact time on the IMI percentage recovery, (c) effect of concentration on the IMI percentage recovery, and (d) effect of the Cr-MOF/polymer composite dose on the IMI percentage recovery.

interactions, such as hydrogen bonding between the composite and the target pesticide functional groups.

3.6. Adsorption equilibrium

Isotherm analysis was conducted on the equilibrium adsorption data. This represents a crucial tool for optimizing the adsorption processes and also understanding the adsorbate and adsorbent (Cr-MOF/polymer composite) interaction.[52] Langmuir and Freundlich models were employed, utilizing their nonlinear forms, as shown in Fig. 9(b).[53] While impressive R^2 values (0.98, 0.99) were obtained for the Langmuir and Freundlich isotherms regarding IMI, it is important to note that the determination of the optimal isotherm model requires close alignment of q_{ecal} and q_{eexp} data along with higher R^2 values, as shown in Table 2.[54] In the case of IMI, the Langmuir isotherm's calculated q_e value was 66.91 mg g^{-1}, while the experimental q_e value was 55.7 mg g^{-1}. These values are not in close agreement, indicating that the Langmuir model was less suitable for describing the adsorption of IMI. In contrast, the Freundlich isotherm provided a better fit, demonstrating a high R^2 value and a more favorable match between the experimental and calculated q_e values. The high K_f value in the Freundlich model suggested the strong adsorption capacity of the composite. Furthermore, the $1/n$ value, which falls between 0 and 1, also supports physisorption as the dominant mechanism for IMI adsorption. The constant 'n' exceeding unity, due to the $1/n$

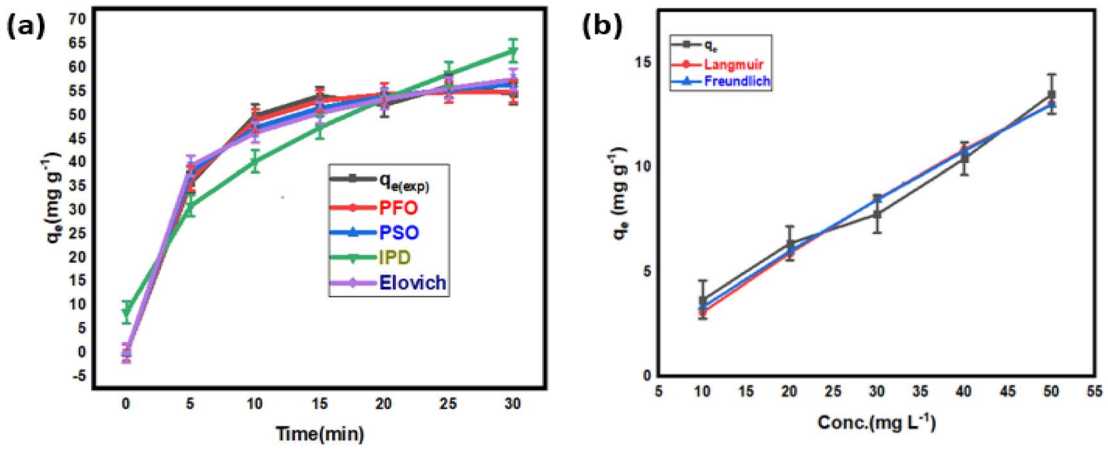

Fig. 9 Nonlinear fitting of the PFO, PSO, Elovich and intraparticle diffusion kinetic models (a), and nonlinear fitting of the Freundlich and Langmuir models (b) for the adsorption of IMI on Cr-MOF/polymer composite.

Table 1 Kinetic variables obtained using the pseudo-first-order, pseudo-second-order, Elovich and intraparticle diffusion models for IMI on Cr-MOF/polymer composite

Model	Adsorption kinetic parameter	Value
Pseudo-first-order kinetic	R^2	0.996
	K_1 (min^{-1})	0.218
	q_e (mg g^{-1})	55.2
	χ^2	1.86
Pseudo-second-order kinetic	R^2	0.988
	K_2 (g mg^{-1} min^{-1}) $\times 10^{-2}$	0.005
	q_e (mg g^{-1})	62.63
	χ^2	5.048
Elovich	R^2	0.98
	α (mg g^{-1} min^{-1})	93.27
	β (g mg^{-1})	0.094
	χ^2	9.7
Intraparticle diffusion	R^2	0.866
	K_{diff} (mg g^{-1} min$^{1/2}$)	10.05
	C (mg g^{-1})	8.53
	χ^2	64.84
Experimental q_e (mg g^{-1})		55.16

value being less than 1, further confirmed the sorbent's effectiveness, highlighting its suitability for IMI adsorption.[55] The adsorption capacity of the Cr-MOF/polymer composite (q_e = 55.16 mg g^{-1}) was compared with other reported adsorbents, such as cetyltrimethyl ammonium-modified bentonite (q_e = 3.33 mg g^{-1}), sodium alginate combined with peanut husk (q_e = 14.9 mg g^{-1}), and silver@graphene oxide nanocomposite (q_e = 25.7 mg g^{-1}).[46,56,57] Based on these comparisons, it could be concluded that the Cr-MOF/polymer composite demonstrated a significantly higher adsorption capacity and showed it could serve as a suitable adsorbent for the removal of IMI from fish samples.

3.7. Reuse of the Cr-MOF/polymer composite

This study assessed the regeneration efficiency of the Cr-MOF/polymer composite for IMI through multiple adsorptions–desorption cycles using eqn (3).

$$\text{Regeneration efficiency } (\%) = \frac{\text{amount of the analyte desorbed during desorption}}{\text{initial amount of analyte adsorbed}} \times 100 \quad (3)$$

Initially, the regeneration efficiency for IMI was high at 98.6%, but it gradually decreased, stabilizing at 86.9% after six cycles, as shown in Fig. 10(a). When applied to fish, the initial regeneration efficiency for IMI was 65.4%, which dropped to 42.5% after six cycles. These results highlight the sorbent's durability and its potential for practical applications, due to its stable structural properties and effective surface functionality that support efficient adsorption and desorption processes, as shown in Fig. 10(b). These results highlight the durability of the Cr-MOF/polymer composite, as its remarkable stability and

Table 2 Adsorption variables obtained using the Freundlich and Langmuir models for IMI on the Cr-MOF/polymer composite

	Langmuir				Freundlich			
	q_m (mg g^{-1})							
Nonlinear modeling	Cal.	Exp.	K_L	R^2	K_F	$1/n$	R^2	$q_{e(cal)}$
Imidacloprid	66.91	55.16	0.004	0.987	2.05	0.8453	0.991	56

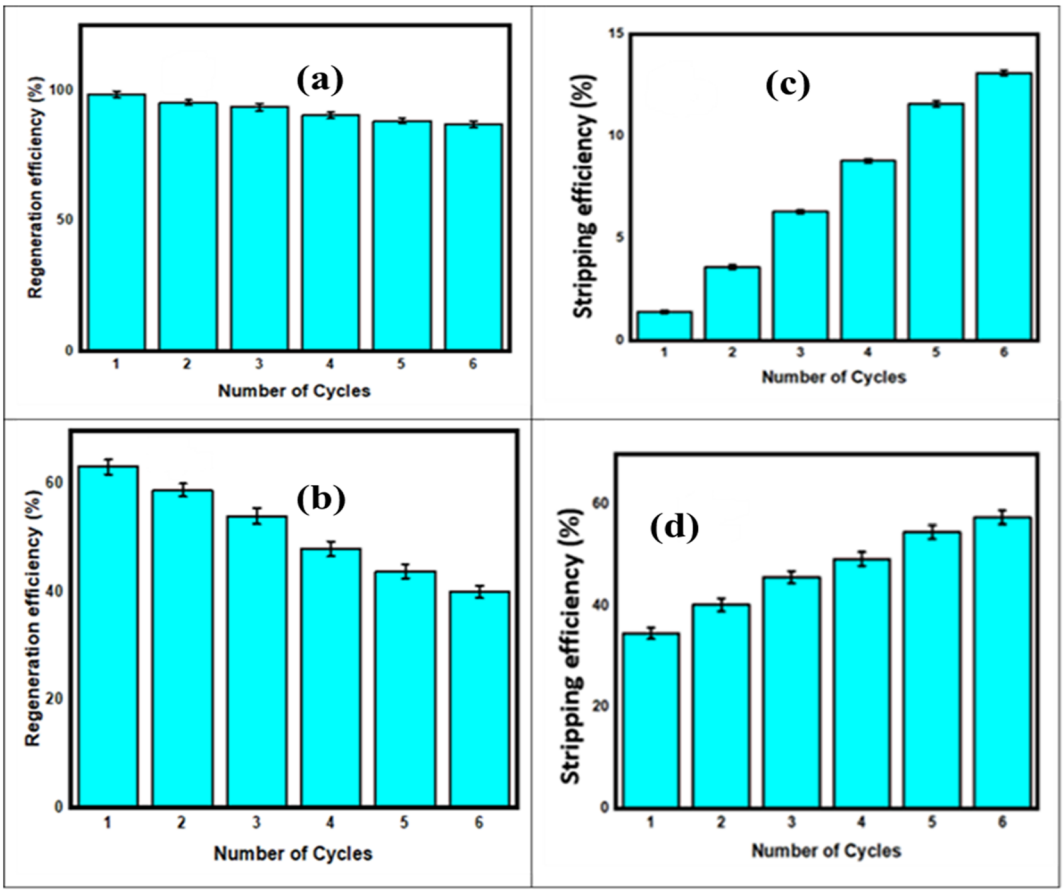

Fig. 10 (a) Regeneration efficiency of the Cr-MOF/polymer composite for spiked samples in water. (b) Stripping efficiency calculated using standard solutions of IMI in water. (c) Regeneration efficiency of the Cr-MOF/polymer composite for spiked samples in fish. (d) Stripping efficiency of the Cr-MOF/polymer composite for six continuous cycles for IMI in fish.

efficiency make it highly sustainable for practical usage in various analytical settings.[58] Similarly, the Cr-MOF/polymer composite stripping efficiencies for IMI highlight the effectiveness of the stripping processes in desorbing the target analyte (IMI) from the surface of the Cr-MOF/polymer composite. The stripping efficiency was calculated using eqn (4).

$$\text{Stripping efficiency } (\%) = \frac{\text{amount of the analyte stripped from the adsorbent}}{\text{total amount of the analyte desorbed after adsorption step}} \times 100 \quad (4)$$

In the next step, 50 mg L^{-1} IMI solutions were prepared in flasks with pH values ranging from 3 to 10, adjusted using 0.1 M HCl and NaOH solutions. Then, 10 mL IMI solution was thoroughly mixed with 50 mg Cr-MOF/polymer composite and shaken on an orbital shaker for 20 min. Afterwards, the absorbance of the IMI solutions at different pH levels was measured at 270 nm. The desorption percentages for IMI ranged from 1.4% to 13.1%, with lower desorption efficiencies (*e.g.*, 1.4%) suggesting stronger binding between the sorbent and analyte, while higher efficiencies (*e.g.*, 13.1%) indicated more efficient desorption, as shown in Fig. 10(c). The desorption rates for IMI varied from 42.5% to 65.4%, with lower efficiencies indicating challenges in pesticide removal, and higher efficiencies pointing towards effective desorption due to weak interactions or favorable conditions. These findings reinforce the Cr-MOF/polymer composite's reusability and efficiency, making it useful for various applications, as illustrated in Fig. 10(d).

3.8. Method validation

In the present research, we investigated the adsorption of IMI on a Cr-MOF/polymer composite and thoroughly evaluated the analytical execution of the developed method. HPLC was utilized to authenticate the adsorption of IMI on the sorbent and also to determine the limit of detection and as well as the limit of quantification for the target pesticide. These values were calculated based on the signal-to-noise ratio from the HPLC data, with the LOD found to be 0.004 μg g^{-1} and the LOQ 0.012 μg g^{-1}. The method's linear range, determined using concentration levels from 0.0014 to 5 μg mL^{-1}, was 0.0014–5 μg mL^{-1}. The method's precision was rigorously evaluated through intraday and interday analyses, yielding relative standard

deviation (RSD) values of 3.29% ($n = 7$), 3.36% ($n = 7$), and 3.48% ($n = 7$), indicating excellent precision. These RSD values were determined at concentrations of 0.01, 0.05, 0.1, 1, and 10 μg mL^{-1}, confirming the reliability of the method. To assess the method's applicability in practical scenarios, fish samples spiked with IMI at concentrations of 1, 5, and 25 μg L^{-1} were tested, resulting in high recovery percentages of 98.6% ± 3.78% ($n = 5$) for IMI. The chromatogram showed a prominent peak at 1.5 min corresponding to the retention time of IMI, as illustrated in Fig. 11. Initially, the pesticide was not detected in the non-spiked real sample. The HPLC chromatogram in Fig. 11(a) displays the chromatogram of the fish sample spiked with the standard IMI. The MOF composite was then used to adsorb the pesticide from the spiked sample (according to the procedure described in Section 2.7). The desorption of IMI from the Cr-MOF/polymer composite is shown in the HPLC chromatogram in Fig. 11(b). Comparison of both chromatograms revealed that the pesticide was effectively adsorbed from the spiked fish samples, allowing easy determination. Furthermore, an enrichment of the pesticide was also observed, as could be noticed from the peak height of IMI in both chromatograms. The performance of the Cr-MOF/polymer composite developed in this study was also compared with other sorbents reported in the literature (Table 3), demonstrating superior percentage recoveries for IMI (98.6%).

3.9. Comparative study

A comprehensive literature review was performed to compare the efficacy of the Cr-MOF/polymer composite with conventional methods for removing IMI in different matrixes (Table 3). Among the various sorbents evaluated, such as UiO-66-NH_2, C_{18}, activated charcoal, primary and secondary amines, polyvinyl poly pyrrolidone, molecularly imprinted polymer, and covalent organic frameworks, the Cr-MOF/polymer composite demonstrated exceptional efficiency for IMI removal, presenting a sustainable solution for target pesticide management. With good versatility for capturing active compounds, the Cr-MOF/polymer composite exhibited a low LOQ (0.012 μg g^{-1}) for IMI compared to other sorbents like activated charcoal, C_{18}, primary secondary amine, and a covalent organic framework, which had values of 0.05 mg kg^{-1} and 0.018 mg kg^{-1}, 33 μg kg^{-1}, 17 ng mL^{-1} and respectively. Furthermore, the developed Cr-MOF/polymer composite displayed superior percentage recoveries for IMI (98.6%) compared to UiO-66-NH_2, activated

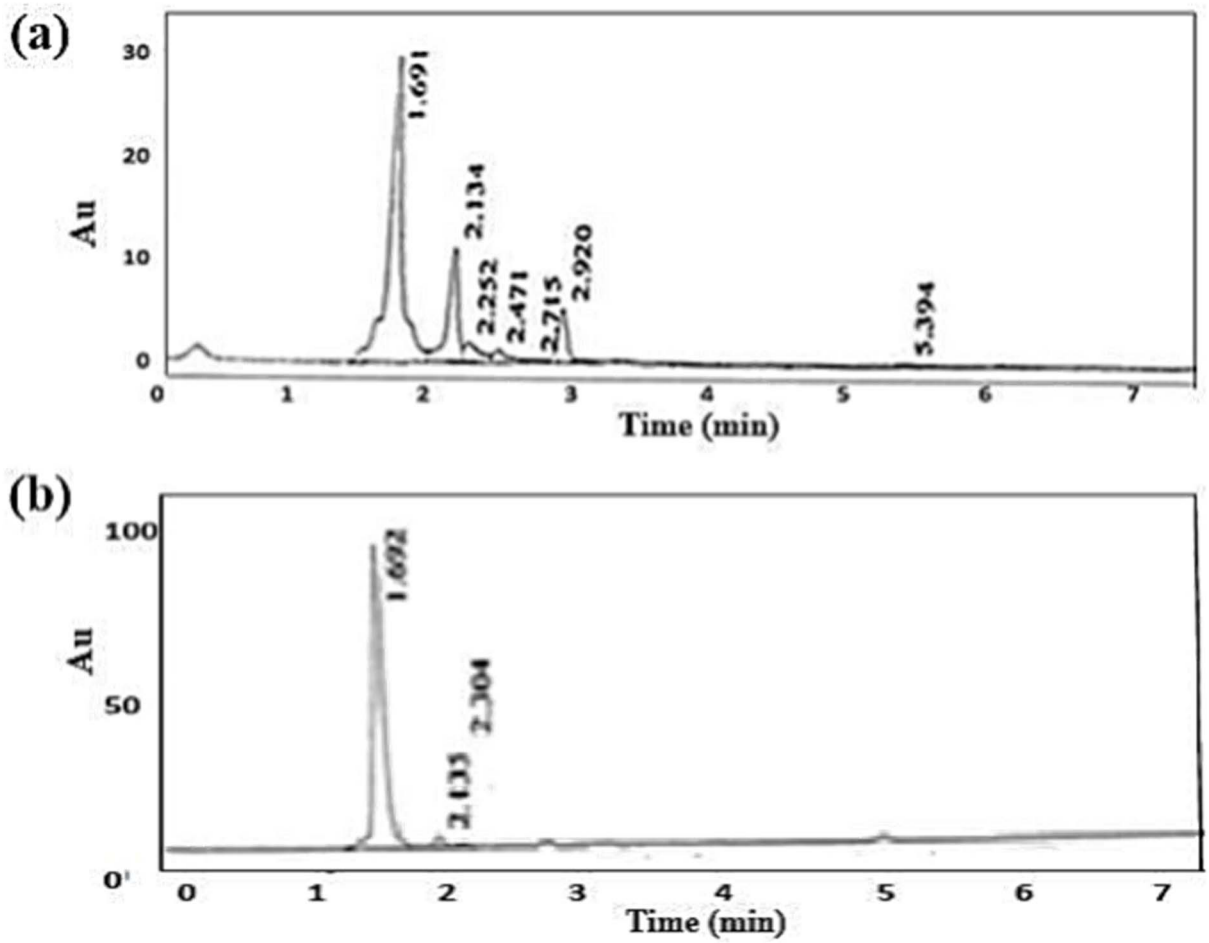

Fig. 11 (a) Chromatogram of the fish sample spiked with the standard IMI. The chromatogram presented in (b) was obtained following the desorption of IMI from Cr-MOF/polymer composite after DSPME.

Table 3 Comparison of the performance of various sorbents and the Cr-MOF/polymer composite in this work for determining imidacloprid[a]

No.	Sample matrix	Analyte	Sorbent	Method	LOQ ($\mu g\ kg^{-1}$)	RSD ($n = 5$)	Recovery%	Ref.
1	Strawberry	IMI	UiO-66-NH_2			7.7	87	59
2	Cucumber	IMI	C18	QuEChERS	18	≤9	98.12	60
3	Tomato	IMI	Activated charcoal	Ultrasound-assisted MSPD	50	≤20	55–140	51
4	Tea	IMI	Primary secondary amine	Modified QuEChERS	0.36	7.4	93.5	61
5	Tea	IMI	Polyvinyl polypyrrolidone	DSPE	0.47	5.7	86	62
6	Pistachio	IMI	Primary secondary amine	Modified QuEChERS-LC-MS/MS	5.0	3.1–6.4	97–108	63
7	Pistachio	IMI	Primary secondary amine	QuEChERS-HPLC-UV	33	<12	70.37–89.80	64
8	Rice	IMI	Molecularly imprinted polymer	MIP-MSPD-LC-MS/MS	8	4.5–5.9	85.2–91.5	65
9	Fruit juice	IMI	Covalent organic framework	FPSE-HPLC-MS-MS	17	4.3	57	66
10	Fish	IMI	Cr-MOF/polymer composite	DSPME	12	3.78	98.6	Current study

[a] MSPD = matrix solid-phase dispersion, DSPE = modified dispersive solid-phase extraction, DSPME = dispersive solid-phase microextraction, QuEChERS = quick, easy, cheap, effective, rugged, and safe. FPSE = fabric phase sorptive extraction.

charcoal, primary secondary amine, polyvinyl poly pyrrolidone, molecularly imprinted polymer and covalent organic framework, further emphasizing its potential as a promising adsorbent for IMI and effective management, presenting enhanced performance for food safety maintenance.

3.10. Conclusion

In conclusion, this study successfully developed and validated a Cr-MOF/polymer composite for the efficient removal and detection of imidacloprid (IMI) in fish samples. The synthesized Cr-MOF/polymer composite consists of a Cr-MOF with a functional monomer having a high absorption selectivity toward IMI in the fish sample matrix. FTIR analysis confirmed the successful formation of the Cr-MOF/polymer composite through the presence of characteristic functional groups, such as nitrile, ester, and ether groups, in the composite's spectrum. SEM images revealed a spherical morphology, with the elemental composition dominated by carbon, followed by oxygen and chromium. HPLC confirmed the sorbent's excellent ability to adsorb IMI, with LOD and LOQ values of 0.004 $\mu g\ g^{-1}$ and 0.012 $\mu g\ g^{-1}$, respectively. The method also achieved a high recovery rate of 98.6% ± 3.78% across a wide linear range of 0.0014–5 $\mu g\ mL^{-1}$, reinforcing the reliability and effectiveness of the approach.

The Cr-MOF/polymer composite's exceptional adsorption capacity can be attributed to hydrogen bonding interactions with the target analyte. These findings were supported by the Freundlich isotherm model and PFO kinetics, which describe the adsorption process well. Additionally, the Cr-MOF/polymer composite showed consistent performance across multiple adsorption cycles, highlighting its potential as a sustainable and effective solution for removing IMI in food safety applications. This work not only advances the field of analytical chemistry but can also contribute to improving food safety by providing a reliable method for detecting and adsorbing pesticide contamination from food products.

Data availability

All the data used in the current study are available upon reasonable request. Furthermore, most of the data are already presented in the manuscript.

Conflicts of interest

There are no conflicts to declare.

Acknowledgements

This work was supported and funded by the Deanship of Scientific Research at Imam Mohammad Ibn Saud Islamic University (IMSIU) (grant number IMSIU-DDRSP2502).

References

1 N. Ahmed, M. A. Sheikh, M. Ubaid, P. Chauhan, K. Kumar and S. Choudhary, *Measurement: Food*, 2024, 100163.
2 M. C. Ogwu and O. A. Ogunsola, in *Food Safety and Quality in the Global South*, Springer, 2024, pp. 263–298.
3 L. Sun, Z. Jiang, B. Yuan, S. Zhi, Y. Zhang, J. Li and A. Wu, *Chem. Eng. Res. Des.*, 2021, **174**, 71–78.
4 S. A. Siddiqui, S. Singh, N. A. Bahmid and A. Sasidharan, *Heliyon*, 2024, **10**(8), e29066.
5 N. An, T. Chen, J. Zhang, G. Wang, M. Yan and S. Yang, *Small Methods*, 2024, **8**, 2300910.
6 V. Menconi, E. Lazzaro, M. Bertola, L. Guardone, M. Mazzucato, M. Prearo, E. Bilska-Zajac, L. Cortinovis, A. Manfrin and G. Arcangeli, *Animals*, 2023, **13**, 3793.

7 A. G. Tacon, R. T. Coelho, J. Levy, T. M. Machado, C. R. Neiva and D. Lemos, *Reviews in Fisheries Science & Aquaculture*, 2024, **32**, 211–305.
8 M. Khairy, M. A. B. Aissa, A. Modwi, E. M. Masoud and N. Raza, *Diamond Relat. Mater.*, 2025, **155**, 112268.
9 N. Raza, S. Razzaq, S. Manzoor, W. Raza, M. Hayat and F. K. Algethami, Emulsifiable neonicotinoid pesticide concentrate, *US Pat.*, Imam Mohammad Ibn Saud Islamic University, 12274265, 2025.
10 K. Aziz, N. Raza, N. Kanwal, M. Khairy, Y. Ahmadi and K.-H. Kim, *Mater. Horiz.*, 2025, DOI: 10.1039/D5MH00627A.
11 T. Wei, J. Y. Leung and T. Wang, *Sci. Total Environ.*, 2024, **920**, 170960.
12 M. Banaee, C. R. Multisanti, F. Impellitteri, G. Piccione and C. Faggio, *Comp. Biochem. Physiol., Part C: Toxicol. Pharmacol.*, 2024, 110042.
13 R. Sangaraju, R. Kumar, T. Huynh and S. N. Sinha, *Pesticide Effects on Human Health and Pest Management*, IntechOpen, 2024, DOI: 10.5772/intechopen.1006807.
14 N. Abbas, M. Hayat, H. Fatima, S. Manzoor, S. Nawaz, F. Mabood, G. Yasmean, A. Majeed and S. Manzoor, *Sep. Sci. Technol.*, 2021, **56**, 518–526.
15 Z. L. Mota, I. A. Díaz, A. E. Martínez-Ávila, M. Otero-Olvera, D. Leyva-Ruíz, L. Aponte-Pineda, S. Rangel-Duarte, J. Pacheco-Aguilar, A. Amaro-Reyes and J. Campos-Guillén, *Environments*, 2024, **11**, 196.
16 F. Wu, S. Zhang, H. Li, P. Liu, H. Su, Y. Zhang, B. W. Brooks and J. You, *Environ. Sci. Technol.*, 2024, **58**(22), 9548–9558.
17 K. Aziz, A. Naz, N. Raza, S. Manzoor and K.-H. Kim, *Environ. Res.*, 2024, **247**, 118256.
18 J. Lu, Z. Zhang, X. Lin, Z. Chen, B. Li and Y. Zhang, *Food Control*, 2022, **131**, 108395.
19 Y. Lei, Y. Luo, N. Fang, Y. Li, X. Wang, H. He, J. Jiang, J. Yu, C. Zhang and X. Zhao, *Agronomy*, 2023, **13**, 1076.
20 İ. Yıldırım and U. Çiftçi, *Environ. Monit. Assess.*, 2022, **194**, 570.
21 Z. Ali, N. Raza, M. Hayat, L. Khezami, M. Khairy, E. A. Almuqri, N. S. Basher, H. Parveen and A. A. Chaudhary, *Frontiers in Nanotechnology*, 2024, **6**, 1516133.
22 Y. Zheng, J. Wang, H. Huang, Y. Ma and X. Zhao, *Trends Food Sci. Technol.*, 2024, 104449.
23 X. He, W. Ji, S. Xing, Z. Feng, H. Li, S. Lu, K. Du and X. Li, *Talanta*, 2023, 125283.
24 D. A. V. Medina, A. T. Cardoso, E. V. S. Maciel and F. M. Lanças, *TrAC, Trends Anal. Chem.*, 2023, **165**, 117120.
25 S. Perveen, A. Hol, J. A. Baig, S. T. H. Sherazi, K. Akhtar, S. Hussain and F. Abbasi, *J. Anal. At. Spectrom.*, 2024, **39**, 2884–2892.
26 M. Hayat, S. Manzoor, H. Raza, M. I. Khan, A. Shanableh, M. Sajid, T. M. Almutairi and R. Luque, *Chemosphere*, 2023, **320**, 137835.
27 M. Z. Momčilović, M. S. Ranđelović, M. Purenović, A. E. Onjia, B. M. Babić and B. Z. Matović, *Desalin. Water Treat.*, 2014, **52**, 7306–7316.
28 Q. Zhou, Y. Ding and J. Xiao, *Anal. Bioanal. Chem.*, 2006, **385**, 1520–1525.
29 F. Yin, F. Xu, K. Zhang, M. Yuan, H. Cao, T. Ye, X. Wu and F. Xu, *Food Chem.*, 2021, **364**, 130216.
30 M. E. Badawy, A. E. S. M. Marei and M. A. El-Nouby, *Sep. Sci. plus*, 2018, **1**, 506–519.
31 A. Mandal, N. Singh and L. Nain, *J. Environ. Sci. Health, Part B*, 2017, **52**, 671–682.
32 L. Liu, T. Feng, C. Wang, Q. Wu and Z. Wang, *J. Sep. Sci.*, 2014, **37**, 1276–1282.
33 C. Negro, H. Martinez Perez-Cejuela, E. F. Simó-Alfonso, J. M. Herrero-Martínez, R. Bruno, D. Armentano, J. s. Ferrando-Soria and E. Pardo, *ACS Appl. Mater. Interfaces*, 2021, **13**, 28424–28432.
34 A. A. Fathi, S. M. Sorouraddin, M. R. A. Mogaddam and M. A. Farajzadeh, *Microchem. J.*, 2023, **187**, 108427.
35 L. Geng, J. Huang, M. Fang, H. Wang, J. Liu, G. Wang, M. Hu, J. Sun, Y. Guo and X. Sun, *Food Chem.*, 2024, 140330.
36 Y. Ban, Y. Li, X. Liu, Y. Peng and W. Yang, *Microporous Mesoporous Mater.*, 2013, **173**, 29–36.
37 T. Wang, J. Tan, S. Xu, Y. Li and H. Hao, *Green Process. Synth.*, 2023, **12**, 20230065.
38 L. Gao, D. Qin, Z. Chen, S. Bai, N. Du, C. Li, Q. Hao and P. Wang, *J. Sep. Sci.*, 2022, **45**, 896–907.
39 T. Encarnação, D. Santos, S. Ferreira, A. J. Valente, J. Pereira, M. Campos, H. D. Burrows and A. A. Pais, *Bull. Environ. Contam. Toxicol.*, 2021, **107**, 131–139.
40 M. Sajjad, R. Almufarij, Z. Ali, M. Sajid, N. Raza, S. Manzoor, M. Hayat and E. A. Abdelrahman, *Food Chem.*, 2024, **430**, 137092.
41 S. Manzoor, J. F. Garcia, K. H. Shah, M. I. Khan, N. Abbas, H. Raza, S. Mubarik, M. Hayat, A. Iram and A. Yar, *Catalysts*, 2022, **13**, 65.
42 H. Motaghi, P. Arabkhani, M. Parvinnia and A. Asfaram, *Sep. Purif. Technol.*, 2022, **284**, 120258.
43 A. Saleem, M. S. Shifa, R. T. Rasool, I. Qureshi, S. A. Buzdar, M. M. Alam, S. Batool, G. A. Ashraf and M. A. Khan, *Ceram. Int.*, 2024, **50**, 11639–11649.
44 M. Tsubaki and N.-T. Yu, *Proc. Natl. Acad. Sci. U. S. A.*, 1981, **78**, 3581–3585.
45 B. Hashemi, P. Zohrabi, N. Raza and K.-H. Kim, *TrAC, Trends Anal. Chem.*, 2017, **97**, 65–82.
46 F. Ishtiaq, H. N. Bhatti, A. Khan, M. Iqbal and A. Kausar, *Int. J. Biol. Macromol.*, 2020, **147**, 217–232.
47 A. Assafi, Y. A. E. H. Ali, R. S. Almufarij, L. Hejji, N. Raza, L. P. Villarejo, B. Souhail, A. Azzouz, E. A. Abdelrahman and E. Rodríguez-Castellón, *Heliyon*, 2023, **9**(11), e22001.
48 M. Hayat, S. Manzoor, N. Raza, H. Raza, A. Javid, Z. Ali, M. I. Khan, F. K. Algethami, N. AlMasoud and T. S. Alomar, *Food Chem.*, 2025, **465**, 141967.
49 G. Franceschini and S. Macchietto, *Chem. Eng. Sci.*, 2008, **63**, 4846–4872.
50 M. Hayat, N. Raza, U. Jamal, S. Manzoor, N. Abbas, M. I. Khan, J. Lee, R. J. Brown and K.-H. Kim, *J. Ind. Eng. Chem.*, 2022, **109**, 202–209.
51 E. O. Dos Santos, J. O. Gonzales, J. C. Ores, L. C. Marube, S. S. Caldas, E. B. Furlong and E. G. Primel, *Food Chem.*, 2019, **297**, 124926.

52 J. Li, X. Wang, G. Zhao, C. Chen, Z. Chai, A. Alsaedi, T. Hayat and X. Wang, *Chem. Soc. Rev.*, 2018, **47**, 2322–2356.
53 J. Imanipoor, M. Mohammadi, M. Dinari and M. R. Ehsani, *J. Chem. Eng. Data*, 2020, **66**, 389–403.
54 M. Hayat, S. Manzoor, N. Raza, A. Abbas, M. I. Khan, N. Elboughdiri, K. Naseem, A. Shanableh, A. M. Elbadry and S. Al Arni, *ACS Omega*, 2022, **7**, 41437–41448.
55 S. Manzoor, M. Hayat, H. Raza, N. Elboughdiri, M. I. Khan, Z. Ali, A. Javed, N. Raza, F. Abdulaziz and A. Shanableh, *Environ. Sci.: Water Res. Technol.*, 2024, **10**, 2162–2176.
56 S. K. Jain, N. A. Shakil, A. Dutta, J. Kumar and M. K. Saini, *J. Environ. Sci. Health, Part B*, 2017, **52**, 326–337.
57 M. Keshvardoostchokami, P. Bigverdi, A. Zamani, A. Parizanganeh and F. Piri, *Environ. Sci. Pollut. Res.*, 2018, **25**, 6751–6761.
58 M.-A. Gatou, I.-A. Vagena, N. Lagopati, N. Pippa, M. Gazouli and E. A. Pavlatou, *Nanomaterials*, 2023, **13**, 2224.
59 Y. Xu, X. Li, W. Zhang, H. Jiang, Y. Pu, J. Cao and W. Jiang, *Food Chem.*, 2021, **344**, 128650.
60 M. F. Abdel-Ghany, L. A. Hussein and N. F. El Azab, *J. AOAC Int.*, 2017, **100**, 176–188.
61 Y. Zhang, Q. Zhang, S. Li, Y. Zhao, D. Chen and Y. Wu, *Food Chem.*, 2020, **329**, 127159.
62 F. Wang, S. Li, H. Feng, Y. Yang, B. Xiao and D. Chen, *Food Chem.*, 2019, **275**, 530–538.
63 M. Faraji, R. Noorbakhsh, H. Shafieyan and M. Ramezani, *Food Chem.*, 2018, **240**, 634–641.
64 V. Mahdavi, Z. Garshasbi, M. M. Farimani, M. Farhadpour and H. Y. Aboul-Enein, *Biomed. Chromatogr.*, 2020, **34**, e4747.
65 L. Chen and B. Li, *J. Chromatogr. B*, 2012, **897**, 32–36.
66 M. M. Daghi, M. A. Farajzadeh, A. Abbasalizadeh, M. R. A. Mogaddam and J. Abolhasani, *Microchem. J.*, 2025, **208**, 112355.